Coordination of physiological traits involved in drought-induced mortality of woody plants

Mencuccini Maurizio[1,2,6], Minunno Francesco[3], Salmon Yann[1], Martínez-Vilalta Jordi[4,5], Hölttä Teemu[3]

[1] School of GeoSciences, University of Edinburgh, Edinburgh EH93FF (UK)

[2] ICREA at CREAF, Cerdanyola del Vallès 08193, Barcelona (Spain)

[3] Department of Forest Science, PO Box 27, University of Helsinki, Helsinki, FI-00014, (Finland)

[4] CREAF, Cerdanyola del Vallès 08193, Barcelona (Spain).

[5] Univ. Autònoma Barcelona, Cerdanyola del Vallès 08193, Barcelona (Spain).

[6] To whom correspondence should be addressed:

School of GeoSciences, University of Edinburgh, Edinburgh EH93FF, Edinburgh (UK); tel: 0044-131-6505432 email: m.mencuccini@ed.ac.uk

Words counts: 6,700

Coordination of physiological traits involved in drought-induced mortality of woody plants

Abstract

- Accurate modelling of drought-induced mortality is challenging. A steady-state model is presented integrating xylem and phloem transport, leaf-level gas exchange and plant carbohydrate consumption during drought development.
- A Bayesian analysis of parameter uncertainty based on expert knowledge and literature review is carried out. The model is tested by combining six data compilations covering 170 species using information on sensitivities of xylem conductivity, stomatal conductance and leaf turgor to water potential.
- The possible modes of plant failure at steady-state are identified (i.e., carbon starvation, hydraulic failure and phloem transport failure). Carbon starvation occurs primarily in the parameter space of isohydric stomatal control, whereas hydraulic failure is prevalent in the space of xylem susceptibility to embolism. Relative to carbon starvation, phloem transport failure occurs under conditions of low sensitivity of photosynthesis and high sensitivity of growth to plant water status, respectively.
- These three failure modes are possible extremes along two axes of physiological vulnerabilities, one characterized by the balance of water supply and demand and the other by the balance between carbohydrate sources and sinks. Because the expression of physiological vulnerabilities is coordinated, we argue that different failure modes should occur with roughly equal likelihood, consistent with predictions using optimality theory.

Key-words: phloem transport, xylem embolism, phloem viscosity, photosynthetic down-regulation, water stress, drought-induced mortality, source-sink relationships, optimality.

Introduction

Mortality of plants as a consequence of drought events has become a major focus of attention recently as a result of reports highlighting severe mortality episodes around the globe (e.g., Allen et al., 2010; Peng et al., 2011). Current process-based models do not adequately represent local and regional mortality, because they have been constructed primarily to represent the fluxes of carbon, water and nutrients and because they have not been calibrated against datasets of severe drought episodes (Powell et al., 2013; McDowell et al., 2013). Consequently, doubts exist as to their capacity to predict shifts in vegetation composition a consequence of increased drought frequency and intensity (e.g., Anderegg et al., 2012, Adams et al., 2013; Xu et al., 2013; Meir et al., 2014).

One central element of uncertainty is given by the lack of detailed understanding of the environmental, ecological and physiological processes leading to mortality (McDowell et al., 2013). The existing datasets which have documented plant mortality paying sufficient attention to some of the underlying physiology (e.g., Adams et al., 2009; Fisher et al., 2010; Anderegg et al., 2012; Hartmann et al., 2013; Mitchell et al., 2013; Poyatos et al., 2013) differ in the emphasis given to different aspects of the mortality process. Partly as a consequence, different interpretations of the main processes affecting mortality have emerged (McDowell et al., 2008; Adams et al., 2009; Sala, 2009; Sala et al., 2010; McDowell & Sevanto, 2010). In addition, biotic interactions can interact significantly with the physiological status of the plants to increase the chances of drought-related mortality (Dobbertin & Rigling 2006; Wermelinger et al., 2008; Galiano et al., 2011; Heiniger et al., 2011; McDowell, 2011; Zweifel et al., 2012; Krams et al., 2012; McDowell et al., 2013).

Being able to avoid death is arguably the most important attribute that living organisms must possess to reach reproductive age and transmit their genes to future generations. A tenable assumption is that, over evolutionary times, plants have adopted strategies that minimise their chances of failing quickly in response to multiple abiotic hazards such as drought (e.g., Anderegg et al., 2013). From this perspective, the threats of mortality caused by failure of the hydraulic transport systems (xylem or phloem) and of starvation caused by lack of carbon can be viewed as possible extremes across a continuum of physiological vulnerabilities (Meir et al., 2014). From an evolutionary perspective, the expression of functional traits might be optimally coordinated to minimise the chance that any one source of mortality risk prevails. If that was not the case, plants would arguably be over-built with respect to the risk posed by individual hazards.

The present work has three main objectives. Firstly, we present a steady-state model that incorporates many of the processes involved in drought-induced mortality, with an emphasis on the interaction between water and carbon fluxes. In the framework proposed by McDowell et al (2008), the central distinction is between length and intensity of drought events, mediated by the degree of isohydric regulation of water potential. Here, we expand that analysis. Secondly, we explore the biological parameter space of the model, which constrains the range of water- and carbon-related processes leading to physiological failure and mortality. Finally, we employ empirical data to test the optimality idea set out above, that mortality risks should be equally likely across species, thanks to the coordination of the relevant functional traits. A steady-state model has distinct advantages compared to time-dependent approaches, because assumptions about poorly known processes (such as thresholds and regulatory dynamics of carbohydrate pools) are avoided and because the number of parameters is small enough that fitting to empirical datasets with quantified uncertainty is possible (Meir et al., 2014). It suits our objective to determine the trait set involved in mortality, rather than predicting the time courses to death.

Description

Model structure

The steady-state model develops a previously published coupled xylem and phloem transport model (Hölttä et al. 2009a). Definitions, symbols, units and choice of values for all the parameters employed in the model are given in Tables 1 and 2 (for the parameters whose values were changed and those that were kept fixed, respectively). A diagrammatic representation of model structure is given in Fig.1, with the represented processes individually numbered. In the two parallel transport systems of the xylem and the phloem, axial hydraulic conductances of all vertical elements are calculated from cross-sectional areas and hydraulic conductivities. Following Minunno et al. (2013), we determined the number of finite elements required to resolve the system's nonlinear responses. We progressively shortened the number of elements of the catena from 100 to 10. For all state variables, the difference in outputs between catenas with 100 and 40 elements was very small. The difference in outputs between catenas with 40 and 10 elements was less than 5%. The final simulations were carried out with 100 elements.

The xylem water pressure at each element is calculated from the water pressure of the element underneath it (for the bottommost element of the catena, this is the soil water potential, Ψ_{soil} in Fig.1) minus the effects of gravity and the viscous pressure losses caused by xylem sap flux (F_{xyl} in Fig.1). For each vertical phloem element, equations of radial water exchange with the xylem (F_{radial} in Fig.1), phloem axial sap flow (F_{ph} in Fig.1), water conservation and solute conservation

are written (Hölttä et al., 2009a). The boundary condition at the bottommost element of the phloem (the 'sink') is such that the sugar unloading rate at the sink maintains a "target" turgor pressure (U_{100} in Fig.1). Different values of this target turgor pressure were employed, with their range given in Fig.S1A. The viscosity of the phloem sap is a function of its sucrose concentration at each element using an equation describing this dependency accurately up to osmotic potentials of about -8 MPa (cf., Morison, 2002 and the green dashed double-arrowed link in Fig.1 linking phloem sucrose osmotic potential c_{ph} with phloem conductance K_{ph}). This is an essential feature of the Hölttä et al. (2009a) model resulting from sucrose being the only solute transported and also the cause for the viscosity increases. It predicts a point of potential vulnerability for the phloem if the system fails to transport all the products of photosynthesis. A very dilute solution minimizes viscosity but requires large volume fluxes, while a very concentrated solution minimizes volume fluxes but increases viscosity. Jenssen et al (2013) showed that this problem leads to an optimal solute concentration that is broadly consistent with the concentrations normally measured in plants under well-watered conditions (cf., Lang (1978) and Hölttä et al., (2009a), for similar arguments). In practice, it translates into a vulnerability curve for the phloem as a function of phloem osmotic potential (Fig.S1B), equivalent to the one for the xylem as a function of xylem water potential. The two main parameters affecting the shape of this phloem vulnerability curve are maximum phloem hydraulic conductance and the type of transported osmoticum.

Simulations are driven only by soil water potential (MPa), while transpiration and photosynthesis do not depend on other environmental variables. For each value of soil water potential, a steady-state solution is first found for the xylem water potential profile, PLC and stomatal conductance, by iterating equations (1) to (5) below plus Darcy's law, until water potential of the uppermost element varies by less than 0.001MPa. The procedure is repeated to find steady-state values of phloem transport rates, photosynthesis and respiration, following an approach similar to the one presented in Hölttä et al. (2009a). The model normally converges very quickly and 500,000 runs take a few hours on a desktop computer.

Xylem vulnerability to cavitation

Xylem conductance is assumed to decrease with decreasing water potential according to (Pammenter & Willigen 1998)

$$k_x = k_{0,x}\left(1 - PLC_i\right) \quad (1)$$

where

$$PLC = \frac{1}{\left(1+\exp\left(A_x\left(\Psi - B_x\right)\right)\right)} \quad (2)$$

In Equation (2), Ψ is 'xylem' water potential at any point in the catena and the parameter B_x can be interpreted as the water potential at which xylem conductance reaches 50% of its maximum value (referred to as P50, Pammenter & Willigen 1998). Parameter A_x represents instead the slope of the relationship, i.e., the gradient of change in PLC with changes in water potential. It has been shown (Cochard 2006, Choat et al., 2012) that these two parameters are related, i.e., plants with vulnerable xylem (i.e., high B_x) also have steep vulnerability curves (high A_x) and vice versa. Two examples of curves drawn with extreme values of A_x and B_x taken from the sampled distribution are given in Fig.S1C. Beyond its sensitivity to xylem water potential, plant conductance in Eqn. (1) also depends strongly on the value of maximum hydraulic conductance $K_{0,x}$.

Transpiration rate and stomatal conductance

Transpiration rate is represented as (e.g., Jarvis & McNaughton 1986)

$$T = g_s T_0 \quad (3)$$

Maximum transpiration rate T_0 is given a fixed value of $2.25*10^{-6}$ m^3 s^{-1} (i.e., 50 mmol m^{-2} s^{-1} for a 25 m^2 tree) and the parameter space of suitable hydraulic values is varied by changing maximum plant hydraulic conductance $K_{0,x}$. Fig.S1D shows how the two most extreme values of the parameter $K_{0,x}$ coupled with T_0 affect plant water potentials, following Darcy's law.

While water flux affects xylem Ψ, leaf Ψ affects stomatal conductance g_s, reducing the chances of extremely low water potentials. Similarly to the case for xylem hydraulic conductance, stomatal conductance declines with plant water potential following a sigmoidal curve:

$$g_s = g_{s,0}\left(1 - PLC_{gs}\right) \quad (4)$$

and

$$PLC_{gs} = \frac{1}{\left(1+\exp\left(A_{gs}\left(\Psi - B_{gs}\right)\right)\right)} \quad (5)$$

where $g_{s,0}$ is set to 1.00 and g_s is constrained to vary in the range $0 \leq g_s \leq 1$ in Eqns. (3) and (4). In Equation (5) above, Ψ is 'leaf' (the top element of the catena) water potential and the parameter B_{gs} can also be interpreted as the leaf water potential at which stomatal conductance reaches 50% of its maximum value (cf., Tuzet et al. (2003) for a representation of the relationship between

photosynthesis and stomatal conductance that responds to leaf Ψ). Two extreme examples of the relationship employed here are given in Fig.S1E.

Photosynthesis rate

Photosynthesis rate is modelled as (Mäkelä et al. 1996)

$$P = P_{\max} \frac{g_s}{g_s + \gamma} f_{ns} \quad (6)$$

where P_{max} is a parameter setting the maximum photosynthesis rate, g_s is the stomatal conductance (in relative units from 0 to 1), γ is a parameter describing the saturation of photosynthesis with respect to stomatal opening, and f_{ns} is a factor accounting for the down-regulation of photosynthesis as a function of the osmotic pressure at the source (not included in Mäkelä et al., 1996). Albeit empirical (cf., von Caemmerer & Farquhar 1981), equation (6) incorporates the effects of stomatal aperture and of sink regulation of photosynthesis (e.g., Paul & Foyer 2001). In a preliminary analysis, we let parameter γ vary, but found that its effect on output variables was very small. We therefore kept it fixed in all analyses at a value of 0.2.

Because photosynthesis occurs at the top of the catena of phloem transport cells (the 'source') and sucrose is assumed to be loaded directly into the phloem, f_{ns} is dependent on the sucrose osmotic pressure of the first phloem cell c_1 at the top of the catena (where c_1 is in MPa). The effect of progressive concentration of the products of photosynthesis is therefore represented as:

$$f_{ns} = \frac{c_{\max} - c_1}{c_{\max}} = 1 - \frac{c_1}{c_{\max}} \quad (7)$$

where c_{max} is the parameter giving the maximum osmotic pressure of the phloem (MPa). If c_1=0, there is no down-regulation (f_{ns}=1); if c_1= c_{max}, photosynthesis is depressed to zero (f_{ns}=0) to avoid further phloem loading. Fig.S1F gives a representation of this relationship using the two extreme values of P_{max} and c_{max} employed. Because of our steady-state assumption, photosynthesis rates and phloem loading rates are equal, unless the plant fails. In additional model runs, we compared this model against a representation of the down-regulation of photosynthesis by leaf water potential using the following formulation for f_{ns}:

$$f_{ns} = \exp(P_{\mathrm{mod}} \Psi) \quad (8)$$

where P_{mod} (P_{mod}> 0) is the parameter setting the direct sensitivity of P_{max} to leaf water potential.

Growth and respiration

Growth and growth respiration are not explicitly separated from maintenance respiration, but we assume that the substrate is partially consumed during its transit along the phloem catena (e.g.,

Dewar, 1993; Cannell & Thornley, 2000). This approach is similar to the idea that 'source' photosynthesis and 'sink' respiration are co-limiting processes, resulting in a near-homeostasis of phloem solute osmotic potential profiles as drought develops (i.e., Thornley & Johnson 1990; Minchin et al., 1993; Minchin & Thorpe 1996; Farrar 1996; Bancal & Soltani, 2002; Bijlsma & Lambers 2000).

The respiration rate R from each element i along the catena of phloem transport is assumed to be constant for values of the osmotic pressure c_i between 0 and c_{min}. Above c_{min} (i.e., for more positive osmotic pressures than c_{min}), R increases linearly as a function of c_i. Therefore:

$$R_i = R_0 = 0.10 \frac{P_{max}}{N}$$

$$R_i = R_0 \frac{c_i}{c_{min}} \qquad (9)$$

For $c_i \beta c_{min}$ and $c_i > c_{min}$, respectively (Fig.S1G). R_0 is the base respiration rate at minimum levels of substrate availability. The central value of R_0 was set at 10% of P_{max} divided by N, the number of elements of the catena. Uncertainty in this parameter was introduced by Monte Carlo sampling of the parameter space (cf., later on). In the baseline scenario, we assumed no direct dependency of respiration on plant water status. In additional simulations (cf., Supplementary Materials, Section C), a direct dependency of respiration on water potential was introduced using an additional parameter, as done above for P_{max}, i.e.:

$$R_i = R_0 \exp(R_{mod} \Psi) \qquad (10)$$

where R_{mod} ($R_{mod} > 0$) is the parameter setting the direct sensitivity of R_0 to water potential.

In the baseline simulations, increased phloem concentrations during drought always lead to increased respiratory losses (cf., Eqn.9 above). The dependency on water potential of Eqn. (10), either alone or in combination with Eqn. (9), allows for the moderating effects of low plant water status on plant respiration when phloem concentrations are high.

Because we assumed a constant sink turgor pressure (see above), each solution for steady-state photosynthesis and respiration resulted in a certain amount of carbohydrates not being employed for respiration and being unloaded at the sink. We refer to this fraction as F_{resid}, the residual flux of transported carbohydrates. This metric is useful as an indicator of carbohydrate availability or potential carbohydrate storage, as it represents the fraction produced in the leaves, transported through the phloem, not respired by the catena and unloaded at the sink.

Definition of modes of failure

Some of the processes represented in the model contain negative feedback loops that tend to stabilize plant performance and avoid run-away failure (red arrows in Fig.1). Two of the processes (drought-induced cavitation in the xylem and viscosity-induced reductions of conductance in the phloem, green arrows in Fig.1) are destabilising feedback loops that can lead to failure. We classified the possible modes of plant failure at steady state as:

1. Hydraulic failure (HF). A combination of parameters was assumed to lead to HF when the calculated rate of xylem hydraulic conductance fell to zero as a result of complete xylem cavitation, i.e.,

   $$K_x=0 \quad (11)$$

2. Carbon starvation (CS). A combination of parameters was assumed to lead to CS when the calculated steady-state rate of photosynthesis was lower than the steady-state rate of respiration by the catena, i.e.,

   $$P<R_{tot} \quad (12)$$

   Because respiration was calculated for each element of the model separately, R_{tot} represents the sum of the N respiratory terms. By definition, $F_{resid}=0$ when $P \leq R_{tot}$.

3. Phloem transport failure (PF). A combination of parameters was assumed to lead to PF when the rate of photosynthesis was greater than the rate at which carbohydrates could be transported out of the leaf as a result of excess phloem viscosity, i.e.,

   $$F_{ph}<P \quad (13)$$

The definitions of such modes of failure need to be interpreted in the narrow sense that is consistent with the use of a steady state model, as opposed to the broader definitions applicable to the field. For example, the definition of CS above should be relaxed to the broader negative carbon balance under prolonged non-steady state conditions, because a negative carbon balance during a short time period does not necessarily lead to failure. Similarly, the narrow criterion of PF for steady state conditions should be relaxed to the broader lack of equilibrium between photosynthesis and phloem transport (and therefore changing storage pools) under non-steady state conditions.

Exploration of parameter space

Of the 17 model parameters, eleven have the potential to affect the likelihood and the mode of plant failure. The behaviour of 11 of these parameters (13 including P_{mod} and R_{mod}) was examined by carrying out a prior parameter uncertainty quantification (van Oijen et al., 2013) to determine the sensitivity of model outputs to uncertainty in the global parameter space, as opposed to

changes in individual parameters (i.e., Beven and Binley, 1992). We defined the prior parameter space based on literature estimates. We examined compilations that summarised hydraulic traits for different biomes and plant functional types (cf., Notes S1). For each compilation, we extracted the range of the main hydraulic parameters to set the limits of our prior distributions. Values of maximum photosynthetic rates were constrained based on values from the GLOPNET database (Wright et al., 2005).

We used log-normal distributions for our sampled parameter space (Table 1 and Hölttä et al., 2009a), with 95% of the values within limits obtained by multiplying and dividing the central estimate by 10. Parameters were generally sampled using univariate log-normals. Multivariate lognormals were sampled using the function mvnorm in the library MASS (Venables & Ripley 2002) in R 3.0.2 (R Development Core Team 2013) for the parameters related to xylem vulnerability curves and for those related to the response of stomatal conductance to water potential. For the first set of parameters (i.e., A_x and B_x and K_x), the covariances ensured that A_x and B_x were positively and curvilinearly related (Cochard 2006; Choat et al., 2012) and that high values of B_x (i.e., values of P50 close to zero) corresponded to high values of xylem K. For the second set of parameters, the covariance ensured that A_{gs} and B_{gs} were similarly positively but loosely related (Manzoni et al., 2013; 2014).

Sampling was repeated 500,000 times. For each of the 500,000 parameter combinations, a drought sequence was imposed on the model plant, starting from a soil water potential of -0.005 MPa and continuing in steps of 0.005 MPa. At each step, the model calculated the steady-state values of all state variables and checked whether the three conditions defining the modes of failure (Eqn. 11, 12 and 13) were encountered. If steady-state values could be found for all state variables and none of those conditions were satisfied (i.e., if $P=F_{ph}>R_{tot}$ and $K_{xyl}>0$), the soil water potential was lowered. This process continued until a value of soil water potential was reached at which one of the conditions above was satisfied. At this point, failure was deemed to have been reached as CS, HF, or PF.

The 500,000 combinations of initial parameter values, output variables and classified modes of failure were screened to eliminate runs that were clearly outside the range of realistic values ('non-behavioural simulations'; Beven and Binley, 1992). This was accomplished by selecting limits to two variables, i.e., leaf water potential and water use efficiency. Runs were given a probability of 1 only if: a) steady-state values of 'leaf' water potentials Ψ at a soil water potential of -0.005 MPa were within the range $-3.0 < \Psi < -0.2$ MPa, and b) the internal water use efficiency (i.e., the ratio of assimilation divided by stomatal conductance) did not decrease between the soil water potential of -0.005 MPa and the critical soil water potential at failure. Alternatively, runs

were given a probability of 0. Condition a) ensured a loose coupling between transpiration rate T and xylem hydraulic conductance, forcing realistic values of water potentials. Condition b) ensured that those parameter combinations resulting in reductions in internal water use efficiency during a drought (caused by, e.g., a combination of stomatal conductance being very insensitive to leaf water potential and photosynthesis rate being very sensitive to calculated sucrose concentrations or leaf water potential) were excluded.

Model sensitivity analyses

To determine the sensitivity of model outputs to input parameters, we conducted a canonical correlation analysis (CCA, Hair et al., 1998). CCA is a multivariate technique allowing the study of the relationships among sets of correlated multiple dependent (model outputs) and independent variables (model parameters, cf., Notes S1 and Table S2). In addition, we determined the sensitivity of the frequency distributions of the three failure modes to the model boundary conditions and carried out additional simulations varying model parameters that were kept fixed for all the other runs (i.e., phloem radial hydraulic conductance, tree height, degree and direction of correlations between stomatal and xylem parameters). Finally, we compared these results with those obtained after introducing a direct dependency of basal respiration rate and/or maximum photosynthetic rate on plant water potential.

Empirical data analysis

To analyse model behaviour, we used studies that reported values of the sensitivity of xylem conductivity to Ψ, of stomatal conductance to leaf Ψ and of leaf turgor to Ψ (Choat et al., 2012; Bartlett et al. 2012; Manzoni et al., 2013; Nardini & Luglio 2014; Klein 2014; Manzoni et al., 2014). Six additional species came from Vilagrosa et al. (2014). The P50 values given by Choat et al. (2012), Vilagrosa et al. (2014), Klein (2014) and Manzoni et al. (2013) were directly equated with B_x. Manzoni et al. (2013) and Klein (2014) directly reported B_{gs}, using stomatal conductance and sap flux data against leaf Ψ. A significant overlap in the species coverage of these two datasets was found, even though absolute values of B_{gs} were frequently different between them. The Manzoni et al. (2014) dataset is an expanded version of the Manzoni et al. (2013) version. Bartlett et al. (2012), Nardini & Luglio (2014) and Vilagrosa et al. (2014) reported Ψ_{tlp} (water potential at turgor loss point, i.e., the Ψ at which leaves, on average, lose turgor). Ψ_{tlp} is an index of plant resistance to water stress and does not directly control the dependency of stomatal conductance to water potential. Estimates of B_{gs} obtained from the relationship between sap flux data and water potentials have similar limitations. Values of Ψ_{tlp} were only assumed proportional

to B_{gs} and the assumption of proportionality between Ψ_{tlp} to B_{gs} was tested in three ways. Firstly, we let the proportionality coefficient between Ψ_{tlp} and B_{gs} vary between 0.3 and 1.0 and we checked whether changes in these coefficients affected our conclusion on the distribution of species values in model parameter space (cf., Notes S2, Tables S4-S5 and Figures S2-S3). Secondly, we checked databases for species with pairs of values of B_{gs} and Ψ_{tlp}. We found 14 species, giving a correlation coefficient of 0.57 ($P<0.05$), confirming that a relationship between the two estimates can be postulated. Thirdly, to avoid systematic biases, we employed additional categorical variables ('dataset' and 'method'), to test the effects of the individual datasets and of the two methods employed to calculate B_{gs}. We crossed these seven data-sets for common species, checked nomenclature, standardised definitions for biome and eliminated duplications for individual species by value averaging. Plants were separated into the groups of angiosperms and gymnosperms. Coupled values of B_x and B_{gs} were found for 243 independent observations and 170 species across all compilations. The relationship between B_x and B_{gs} was tested using a general linear model in R 3.0.2 (R Core Development Team, 2013), using 'dataset', 'biome' and 'plant group' as additional categorical factors.

Results

Sensitivity analyses and distributions of simulations by failure modes

The boundary conditions selecting the 'behavioural' simulations screened out a significant number of parameter combinations (92% in the baseline case). Of the simulations that were retained under the baseline case, 25% resulted in HF, 71% in CS and only 4% in PF. These proportions varied greatly (cf., Table S3) depending on the imposed boundary conditions, especially tree height (varied between 1m and 100m) and radial hydraulic conductance (varied between $2\ 10^{-13}$ and $2\ 10^{-9}$). The parameter that most affected the frequency distributions of the failure modes was the dependency of plant respiration on water potential. Including this additional parameter (varied from $0.1\ 10^{-6}$ to $1\ 10^{-6}$) increased the proportion of HF (from generally <20 to >30%) and PF (from ~5 to >10%) at the expense of CS (from >75 to <60%).

Model output variables showed sensitivity to a range of parameters for the first five canonical variates (cf., Table S2 in Notes S1). Two parameters with opposing effects (i.e., xylem K and the slope of the stomatal response to Ψ) affected almost the entire set of output variables. Plant Failure mode was primarily related to xylem K, the slope of the stomatal response to Ψ and both xylem and stomatal P50.

Distribution of parameters

The general distribution of the input parameters by mode of failure is given in Fig.2. The last columns (in red) are the reference empirical distributions for those parameters for which data were available from the meta-analyses. In general, the distributions obtained for the three failure modes (in black) encompassed the distributions from the empirical compilations (in red). Xylem conductance K_x showed a significant difference ($P<0.001$) in the parameter distribution between the three modes of failure, with higher values for PF than CS. An even more accentuated difference was found for B_x (xylem P50) and A_x, with much higher values found for mode HF, followed by CS and PF ($P<0.001$). Conversely, B_{gs} (stomatal P50) and A_{gs} showed higher values for CS ($P<0.001$), with no difference between HF and PF. PF was characterized by a combination of parameter distributions, i.e., relatively high K_x, low B_x and A_x (both $P<0.001$), large c_{max} ($P<0.001$) and relatively higher c_{min} and sink turgor U. The distributions of the input parameters by mode of failure did not vary by varying the boundary parameters in the sensitivity analysis (data not shown).

The distribution of the main output variables at failure showed (Fig. 3) that soil and leaf Ψ varied across modes of failure, with significantly more negative values for PF ($P<0.001$). This was associated with higher source turgor pressures ($P<0.001$), more negative osmotic potentials (in turquoise, $P<0.001$, as expected for PF by viscosity) and larger turgor drops from leaves to sink ($P<0.001$). Parameter combinations that resulted in HF showed 100% loss of xylem conductance (in turquoise), almost complete stomatal closure and no photosynthesis. Relative to PF, CS was characterised by lower photosynthetic rates at failure (but not by higher cumulative respiration) and lower cumulative residual fraction of transported carbohydrates at the sink (in turquoise, as expected for this mode of failure). The range of soil water potentials at failure did not differ between HF and CS. The distributions of the output variables at failure varied only marginally by varying the boundary parameters (data not shown).

Controls on modes of failure

A plot of xylem P50 versus stomatal P50 separated HF versus CS (Fig.4). HF was characterized by points distributed at the top of the space delimited by B_x (xylem P50), whereas CS was characterized by points distributed on the side of the parameter space characterized by high values of B_{gs} (stomatal P50). Around a diagonal space from top right to bottom left (i.e., from sensitive stomata plus vulnerable xylem to insensitive stomata plus resistant xylem), a relatively wide region of overlap between the two modes of failure was found. Fewer points were found in the left bottom corner of the parameter space. For each of the two modes of failure, plant water

potential at failure depended on parameter combinations. Low (negative values) of xylem P50 resulted in low critical leaf water potentials for the case of HF. Similarly, for the case of CS, low values of stomatal P50 resulted in low critical leaf water potentials.

When the 170 species from the meta-analytical compilations were plotted on the B_x-B_{gs} space (as in Fig.4), the vast majority of the points fell within a region covering the bivariate 99% ranges of these two modes of failure around the main diagonal line (Fig.5). A significant positive relationship was found between xylem P50 and stomatal P50 across all datasets (all $P<0.001$, depending on the assumed relationship between stomatal turgor loss point and B_{gs}, cf., Table 3 and Tables S4-S5 in Notes S2), with a significant negative intercept for the gymnosperms ($P<0.001$), indicating a lower P50 (between about -1.1 and -1.9 MPa) for a fixed stomatal P50. Highly significant effects were also found for 'dataset' (with significant differences for the Vilagrosa dataset, $P<0.001$) and 'biome' (with significant differences for the dry schlerophyllous biome, $P<0.001$). The overall model including stomatal P50, the three categorical variables and their interactions explained between 59 and 60% of the variance (Table 3, S4 and S5). Despite changes in the distribution and linear fits in Fig.5 depending on the assumption made for the conversion between leaf stomatal P50 and Ψ_{tlp}, the bulk of the data points remained in the area of joint overlap between the two bivariate distributions of 99% of the simulations for HF and CS (Figures S2 and S3 in Notes S2).

CS and PF differed for parameter combinations regulating plant carbon source-sink balance. Because multiple parameters affected the photosynthetic and respiratory responses, composite response parameters were calculated for each, following the response curves given in Eqns.9-15. Relative to PF, CS was characterised by parameter combinations leading to a weak regulation of respiration ($-R_0/(U*c_{min}$, i.e., base respiration; degree of respiration down-regulation by osmotic pressure -or water potential- and phloem turgor pressure, cf., Fig. 2) and a strong regulation of photosynthesis ($P_{max} * B_{gs}/c_{max}$, i.e., maximum photosynthesis, sensitivity of stomatal closure to water potential and photosynthetic down-regulation by osmotic pressure -or water potential-) in response to water stress (Fig.6a). Conversely for PF, the combination of parameters regulating carbon fixation, phloem transport and respiration during drought led to a less sensitive regulation of carbon losses and to a more sensitive regulation of the sinks (Fig. 6b). This resulted in combinations leading to PF being situated above the line of carbon supply/demand and those leading to CS being situated below or on it (Fig. 6b).

Discussion

Model structure and major assumptions

The model incorporates many of the interactions among the processes of carbohydrate fixation and transport and water transport and transpiration. By way of comparison, the Sperry et al (1998) model includes a very detailed representation of the linkage between gaseous and liquid water transport processes in the soil and the plant, but the processes linked to C fixation and transport are not represented (cf., Mackay et al., 2012, for an advanced combination of water- and carbon-related processes). Conversely, models by Cannell & Thornley (2000) and Dewar (1993) represent C fixation and allocation using concepts related to source and sink strength, but the biophysical representation of xylem and phloem transport is missing. Finally, the model by De Schepper & Steppe (2010) is close to the approach presented here, but its focus is in simulating short-term (minutes to hours) dynamics. The fundamental feature of this model is to include both stabilizing and de-stabilizing processes for xylem and phloem. In the case of phloem transport, the effect of viscosity on conductance is the main de-stabilizing process (cf., Hölttä et al, 2009), viscosity being a strong nonlinear function of sucrose osmotic concentration (Morison, 2002).

We used a Bayesian approach based on literature information and expert knowledge to analyse parameter and model output distributions. In our case, limits to parameter distributions were set using global compilations of parameter values. In addition, screening criteria were set to create boundaries for the parameter space ('behavioural' values). In Bayesian parlour, we constrained partially informative priors by logical criteria based on expert knowledge. Criterion a) is well supported in the literature (Mencuccini 2003; Martínez-Vilalta et al., 2014). Criterion b) is also regarded as a universal observation.

Co-ordination among modes of failure along water supply-demand axis

A plot of xylem versus stomatal P50 discriminated between HF and CS (McDowell et al., 2008). The distribution of these two modes of failure is delimited by a diagonal space going from combinations of sensitive stomata plus vulnerable xylem to combinations of insensitive stomata and resistant xylem. Inside this diagonal space, both types of failure occurred. The significance of this diagonal space can be understood as follows. Firstly, the variability in xylem conductance and stomatal conductance in relation to water and carbon fluxes depends on parameters that are, at least to some degree, correlated with one another (e.g., A_x, B_x with K_x and A_{gs} with B_{gs}). This reduces the dimensionality of the problem. Indeed our sensitivity analysis (cf., Table S2) showed that failure mode was affected by a number of parameter combinations reflected in the covariances mentioned above. Secondly, one would expect that plants evolved strategies to minimise the relative risks caused by different mortality hazards. Traits that would cause plants

to be situated entirely within the space of only one dominant hazard type would likely be evolutionary unstable. It is possible that different optimal solutions evolved such that different sets of functional traits lead to roughly equal chances of mortality by different processes. For example, levels of xylem PLC were higher than 90% for some of the simulations of CS (Fig.3), while total cumulative F_{resid} were also comparatively higher for simulations of HF (Fig.3). One may expect *a priori* that mortality be brought about by a coincidence of several different processes. Recent experiments directly testing mechanisms of mortality show that a single species can die by different causes depending on the circumstances (Sevanto et al., 2014). It is interesting that the vast majority of the species for which empirical data were available were contained within this diagonal space (Fig.5). This dataset of 170 species covered all major biomes, climate conditions and plant types (Table S1). The significant terms for 'dataset' found in the relationship between B_x and B_{gs} in the meta-analytical compilation suggests that caution is needed when different datasets are combined. However, when tested, we did not find a significant effect of the method employed to estimate B_{gs} (i.e., either from sap flow/conductance measurements or from Ψ_{tlp}) based on three different tests. This finding supports the use of Ψ_{tlp} as an indicator also of stomatal behaviour across species.

Co-ordination among modes of failure along carbon supply-demand axis

A plot of photosynthetic versus respiratory parameters discriminated combinations leading to CS from PF. Interestingly many combinations could lead to both modes of failure. PF was associated with an altered balance between carbohydrate sources (less sensitively regulated in relation to drought) and sinks (more sensitively regulated) (Figure 6). This altered balance produced larger residual carbohydrate fluxes and led to wider carbon safety margins (*sensu* Mitchell et al., 2014). These results suggest that plants in which growth continues at low water potentials may be more likely to suffer CS. *Vice versa*, plants may risk PF when consumption of carbohydrates responds sensitively while stomatal and photosynthetic rates remain high during drought. Interestingly, the proportion of combinations resulting in PF was strongly increased when a direct sink limitation by plant water status was introduced (Table S2).

Evidence for the response of photosynthetic non-stomatal parameters to drought was recently reviewed by Zhou et al (2013). While growth is very sensitive to turgor reductions, the response of respiration to drought is more rarely documented. Duan et al. (2013, 2014) and Ayub et al. (2011) found that leaf dark respiration declined only at the end of severe droughts while Metcalfe et al. (2010) reported increases in stem respiration during drought in a tropical rainforest. The

response of growth to drought is almost never documented (cf., Mitchell et al., 2014 for an exception).

The diagonal 1:1 line of Fig.6b is the line of source/sink balance. CS and PF can both be avoided provided a plant can co-regulate source and sink activity with equal sensitivity during drought. This appears to be possible for some, but not all, parameter combinations (cf., regions of overlap between the two failure modes in Fig.6a). Combinations leading to HF were found well below the 1:1 source/sink balance line of Fig.6b, i.e., in the same region as CS (data not shown). This is because hydraulic regulations of stomatal conductance during drought led to stomatal closure and lower photosynthesis, but not necessarily lower respiration rates. In our model, we assumed that photosynthesis and respiration, but not F_{resid}, were actively controlled by plant water status. In other words, the assumptions in our model are equivalent to the assumption that allocation to carbohydrate storage is a residual term.

It is important to note that CS was affected also by phloem properties, albeit indirectly, via the effects of changed phloem turgor, phloem osmotic potentials and phloem conductance. This is supported by the results of the sensitivity analyses of Table S2 and S3. The osmotic and turgor variables at failure (leaf osmotic pressure at failure, leaf turgor pressure at failure) were affected by a combination of xylem, phloem and gas exchange parameters (Table S2).

Our steady state model constrains the solutions to a space where turgor is kept constant, but phloem transport may also temporarily fail under dynamic conditions by reaching turgor loss for limited but crucial time periods (e.g., McDowell et al. 2013, Sevanto et al. 2014). For example, under drought, low photosynthesis may result in sucrose concentrations barely capable of maintaining a positive turgor pressure.

Non-steady-state behaviour and time scales to mortality

How much would the conclusions drawn on the basis of Figs.5-6 change, had we incorporated non-steady state conditions? It is likely that additional failure modes exist that can only be identified under non-steady state conditions. However, the characterization of these additional modes is prevented by our lack of mechanistic understanding of the underlying processes. In addition, non-steady-state models tend to be parameter-rich and their calibration within known uncertainty margins is difficult. Considering these limitations, a steady-state approach seems a reasonable first approximation. In the context of the variables studied here, the behaviour of a xylem hydraulic capacitor may primarily affect the magnitude of the declines in xylem water potentials, slowing down xylem cavitation and HF. For example, Meinzer et al (2003) showed that diurnal changes in plant water potential and sap flow can be moderated significantly as a

result of the presence of hydraulic capacitors and cavitation of xylem conduits may have temporary moderating effects (cf., Hölttä et al., 2009b). Alternatively, a leaf capacitor may primarily slow down the declines of water potential, thereby reducing stomatal closure and CS.

Dynamic carbohydrate storage under high photosynthetic rates may lower phloem loading and prevent excessive solute concentrations (and viscosity) in the phloem but at the same time, carbohydrate release may prevent dangerously low levels of sugar concentrations and loss of turgor under conditions of long and intense respiratory losses. Empirical data are currently unavailable to help tease out these possibilities.

Incorporating processes resulting in non-steady state conditions may be useful under significant hydraulic disequilibrium between soil and plant. Several causes of hydraulic disequilibrium have been reported (i.e., transient accumulation of solutes, lack of over-night equilibration in plant hydration, continued night-time transpiration; cf., Donovan et al., 2003). Expanding this model to include processes occurring during longer time periods would allow probing the significance of progressive leaf shedding, changing rooting depth and root/shoot ratios, xylem growth and refilling and cavitation fatigue.

Conclusions

The interpretation of mortality given here, of a process occurring along two independent axes representing the dimensions of water supply/demand and carbon supply/demand differs significantly from McDowell et al. (2008), where the primary axis driving mortality was the degree of isohydric/anisohydric regulation of water potential. Stomatal behaviour turns out to be just one component of a strategy that minimizes the risk of three different modes of mortality. A plot of stomatal versus xylem P50 separated out the possible parameter combinations leading to HF from those leading to CS. Conversely, PF could be separated from CS by parameter combinations regulating phloem transport, respiration and photosynthesis. PF occurred especially when growth was assumed to respond sensitively to plant water status while stomatal regulation and photosynthetic down-regulation were limited. Maintaining phloem turgor via regulation of osmotic pressure, and the link between solute concentration and viscosity were crucial in understanding the relative sensitivity of growth and gas exchange to drought. With regard to model validation, this exercise showed that only about half of the parameters currently in the model could be constrained empirically. Some of the remaining parameters (i.e., sink turgor pressure) can be constrained using analogous leaf or root turgor measurements (Mencuccini M., Minunno F., Salmon Y, Poyatos R, Hölttä T, Martínez-Vilalta J., unpublished), however empirical calibration remains difficult for others (e.g., phloem-related parameters).

572

573 ## Acknowledgements

574 FM acknowledges support from the STReSS COST action (FP1106) for short term scientific
575 missions to Edinburgh and Barcelona. MM and YS acknowledge support from NERC (project
576 NE/IO107749/1). This research has been supported by the Spanish Ministry of Economy and
577 Competitiveness through grant CGL2010-16373. We thank the ARC-NZ Vegetation Function
578 Network for supporting the compilation of the Xylem Functional Traits dataset and Brendan
579 Choat and Steven Jansen for granting us access to the data. We thank José Luis Ordóñez for
580 assistance in the preparation of Figure 1. The authors have no conflicts of interest to declare.
581 The insights from five reviewers helped considerably to sharpen the focus of the analysis.

582

583 ## References

584 Adams HD, Guardiola-Claramonte M, Barron-Gafford GA, Villegas JC, Breshears DD, Zou
585 CB, Troch PA & Huxman TE. (2009) Temperature sensitivity to drought-induced tree mortality
586 portends increased regional die-off under global-change-type drought. *Proceedings of the National*
587 *Academy of Sciences, USA* **106**, 7063-7066.
588 Adams H.D., Williams A.P., Xu C., Rauscher S.A., Jiang X. & McDowell N.G. (2013) Empirical
589 and process-based approaches to climate-induced forest mortality models. *Frontiers in Plant Science*
590 **4**, 438. published: doi: 10.3389/fpls.2013.00438.
591 Allen C.D., Macalady A.K., Chenchouni H., Bachelet D., McDowell N., Vennetier M.,
592 Kitzberger T., Rigling A., Breshears D.D. & Hogg E.H. (Ted) *et al.* (2010) A global overview of
593 drought and heat-induced tree mortality reveals emerging climate change risks for forests. *Forest*
594 *Ecology and Management* **259**, 660–684.
595 Anderegg W.R.L., Berry J.A. & Field C.B. (2012b) Linking definitions, mechanisms, and
596 modeling of drought-induced tree death. *Trends Plant Science* **17**, 693–700.
597 Anderegg L.D.L., Anderegg W.R.L. & Berry J.A. (2013) Not all droughts are created equal:
598 translating meteorological drought into woody plant mortality. *Tree Physiology* **33**, 701-712.
599 Ayub G., Smith R.A., Tissue D.T. & Atkin O.K., (2011) Impacts of drought on leaf respiration
600 in darkness and light in *Eucalyptus saligna* exposed to industrial-age atmospheric CO_2 and growth
601 temperature. *New Phytologist* **190**, 1003-1018.
602 Bancal P. & Soltani F. (2002) Source-sink partitioning. Do we need Münch? *Journal of*
603 *Experimental Botany* **53**, 1919-1928.

604 Bartlett M.K., Scoffoni C. & Sack L. (2012) The determinants of leaf turgor loss point and
605 prediction of drought tolerance of species and biomes: a global meta-analysis. *Ecology Letters* **15**,
606 393-405.
607 Bijlsma R.J. & Lambers H. (2000) A dynamic whole-plant model of integrated metabolism of
608 nitrogen and carbon. 2. Balanced growth driven by C fluxes and regulated by signals from C and
609 N substrate. *Plant and Soil* **220**, 71-87.
610 Beven K.J. & Binley A.M. (1992) The future of distributed models: model calibration and
611 uncertainty prediction. *Hydrological Processes* **6**, 279–298.
612 Cannell M.G.R. & Thornley J.H.M. (2000) Modelling the components of plant respiration: Some
613 guiding principles. *Annals of Botany* **85**, 45-54.
614 Choat B., Jansen S., Brodribb T.J., Cochard H., Delzon S., Bhaskar R., Bucci S.J., Field T.S.,
615 Gleason S.M., Hacke U.G. *et al.* (2012) Global convergence in the vulnerability of forests to
616 drought. *Nature* 491, 752-756.
617 Cochard H. (2006) Cavitation in trees. *Comptes Rendus Physique* **7**, 1018-1126.
618 Dewar R. (1993) A Root-Shoot Partitioning Model Based on Carbon-Nitrogen-Water
619 Interactions and Munch Phloem Flow. *Functional Ecology* ***7***, 356-368.
620 Dobbertin M. & Rigling A. (2006) Pine mistletoe (*Viscum album ssp. austriacum*) contributes to
621 Scots pine (*Pinus sylvestris*) mortality in the Rhone valley of Switzerland. *Forest Pathology* **36**, 309-
622 322.
623 Donovan L.A., Richards J.H. & Linton M.J. (2003) Magnitude and mechanisms of disequilibrium
624 between predawn plant and soil water potentials. *Ecology* **84**, 463-470.
625 Duan H., Amthor J.S., Duursma R.A., O'Grady A.P., Choat B. & Tissue D.T. (2013) Carbon
626 dynamics of eucalypt seedlings exposed to progressive drought in elevated [CO_2] and elevated
627 temperature. *Tree Physiology* **33**, 779-792.
628 Duan H., Duursma R.A., Huang G., Smith R.A., Choat B., O'Grady A.P. & Tissue D.T. (2014)
629 Elevated [CO_2] does not ameliorate the negative effects of elevated temperature on drought-
630 induced mortality in *Eucalyptus radiata* seedlings. *Plant Cell and Environment*, 37: 1598-1613.
631 Farrar J. (1996) Regulation of root weight ratio is mediated by sucrose: Opinion. *Plant and Soil*
632 **185**, 13-19.
633 Fisher R., McDowell N.G., Purves D., Moorcroft P., Sitch S., Cox P. et al. (2010) Assessing
634 uncertainties in a second-generation dynamic vegetation model caused by ecological scale
635 limitations. *New Phytologist* **187**, 666–681.

636 Galiano L., Martínez-Vilalta J. & Lloret F. (2011) Carbon reserves and canopy defoliation
637 determine the recovery of Scots pine 4 yr after a drought episode. New Phytologist **190**, 750–
638 759.
639 Gustafson E.J. & Sturtevant B.R. (2013) Modeling forest mortality caused by drought stress:
640 implications for climate change. *Ecosystems* **16**, 60–74.
641 Hair, Jr. J.F., Anderson R.E., Tatham R.L. & Black W.C. (1998) *Multivariate Data Analysis, 5th*
642 *edition ,* Prentice Hall, Inc. London, UK.
643 Hartmann H., Trumbore S., Ziegler W. (2013) Lethal drought leads to reduction in nonstructural
644 carbohydrates (NSC) in Norway spruce tree roots but not in the canopy. *Functional Ecology* **27**,
645 413–427.
646 Heiniger U., Theile F., Rigling A. & Rigling D. (2011) Blue stain infections in roots, stems and
647 branches of declining Pinus sylvestris trees in a dry inner alpine valley in Switzerland. *Forest*
648 *Pathology* **41**, 501-509.
649 Hölttä T., Mencuccini M. & Nikinmaa E. (2009a) Linking phloem function to structure: analysis
650 with a coupled xylem–phloem transport model. *Journal of Theoretical Biology* **259**, 325–337.
651 Hölttä T., Mencuccini M. & Nikinmaa E. (2009b) Capacitive effects of cavitation in xylem
652 conduits: results from a dynamic model. *Plant Cell and Environment* **32**, 10–21.
653 Jarvis P.G. & McNaughton K.G. (1986) Stomatal control of transpiration: scaling up from leaf
654 to region. *Advances in Ecological Research* **15**, 1-49.
655 Jensen K.H., Savage J.A. & Holbrook N.M. (2013) Optimal concentration for sugar transport in
656 plants. *Journal of Royal Society Interface* doi: 10: 20130055.
657 Klein T. (2014) The variability of stomatal sensitivity to leaf water potential across tree species
658 indicates a continuum between isohydric and anisohydric behaviours. *Functional Ecology* **28**: 1313-
659 1320.
660 Krams I., Daukste J., Kivleniece I., Brumelis G., Cibulskis R., Āboliņš-Ābols M., Rantala M.J.,
661 Mierauskas P. & Krama T. (2012) Drought-induced positive feedback in xylophagous insects:
662 Easier invasion of Scots pine leading to greater investment in immunity of emerging individuals.
663 *Forest Ecology and Management* **270**, 147-152.
664 Lang, A. (1978) A model of mass flow in the phloem. *Australian Journal of Plant Physiology,* **5**, 535-
665 546.
666 Mäkelä A., Berninger F. & Hari P. (1996) Optimal control of gas exchange during drought:
667 Theoretical analyses. *Annals of Botany*. **77**, 461-467.

668 Mackay D.S., Ewers B.E., Loranty M.M., Kruger E.L. & Samanta S. (2012) Bayesian analysis of
669 canopy transpiration models: A test of posterior parameter means against measurements. *Journal*
670 *of Hydrology*, **432-433**, 75-83.
671 Manzoni S., Vico G., Katul G., Porporato A. (2013) Biological constraints on water transport in
672 the soil-plant-atmosphere system. *Advances in Water Resources* **51**, 292-304.
673 Manzoni S., Vico G., Katul G., Palmroth S., Porporato A. (2014) Optimal plant water-use
674 strategies under stochastic rainfall. *Advances in Water Resources* **50**: 5379-5394.
675 Martínez-Vilalta J., Poyatos R., Aguadé D., Retana J. & Mencuccini M. (2014) A new look at
676 water transport regulation in plants. *New Phytologist*, **204**: 105-115.
677 McDowell N.G., Pockman W., Allen C., Breshears D., Cobb N., Kolb T., Plaut J., Sperry J.,
678 West A., Williams D. *et al.* (2008) Mechanisms of plant survival and mortality during drought:
679 why do some plants survive while others succumb? *New Phytologist* **178**, 719-739.
680 McDowell N.G. & Sevanto S. (2010) The mechanisms of CS: how, when, or does it even occur
681 at all? *New Phytologist* **186**, 264-266 .
682 McDowell N.G. (2011) Mechanisms linking drought, hydraulics, carbon metabolism, and
683 vegetation mortality. *Plant Physiology* **155**, 1051-1059.
684 McDowell N.G., Fisher R., Xu C., Domec J.C., Höltta T., Mackay D.S. et al. (2013) Evaluating
685 theories of drought-induced vegetation mortality using a multimodel-experiment
686 framework. *New Phytologist* **200**, 304–321.
687 Meinzer F.C., James S.A., Goldstein G. & Woodruff D. (2003) Whole-tree water transport scales
688 with sapwood capacitance in tropical forest canopy trees. *Plant, Cell and Environment* **26**, 1147-
689 1155.
690 Meir P., Mencuccini M. & Dewar R., 2015. Drought-related tree mortality: addressing the gaps in
691 understanding and prediction. *New Phytologist* , doi: 10.1111/nph.13382.
692 Mencuccini M. (2003) The ecological significance of long distance water transport: short-term
693 regulation and long-term acclimation across plant growth forms. *Plant, Cell and Environment* **26**,
694 163-182.
695 Metcalfe D.B., Meir P., Aragão L.E.O.C., Lobo-do-Vale R., Galbraith D., Fisher R.A. et al.
696 (2010) Shifts in plant respiration and carbon use efficiency at a large-scale drought experiment in
697 the eastern Amazon. *New Phytologist* **187**, 608-621.
698 Minchin P.E.H., Thorpe M.R. & Farrar J.F. (1993) A simple mechanistic model of phloem
699 transport which explains sink priority. *Journal of Experimental Botany* **44**, 947-955.
700 Minchin P.E.H. & Thorpe M.R. (1996) What determines carbon partitioning between competing
701 sinks? *Journal of Experimental Botany,* **47** (Special Issue), 1293-1296.

Minunno F., van Oijen M., Cameron D.R. & Pereira J.S. (2013) Selecting parameters for Bayesian calibration of a process-based model: a methodology based on canonical correlation analysis. *Journal on Uncertainty Quantification* **1**, 370-385.

Mitchell P.J., O'Grady A.P., Tissue D.T., White D.A., Ottenschlaeger M.L. & Pinkard E.A. (2013) Drought response strategies define the relative contributions of hydraulic dysfunction and carbohydrate depletion during tree mortality. *New Phytologist* **197**, 862–872.

Mitchell P.J., O'Grady A.P., Tissue D.T., Worledge D., Pinkard E.A. (2014) Co-ordination of growth, gas exchange and hydraulics define the carbon safety margin in tree species with contrasting drought strategies. *Tree Physiology* **34**: 443-458.

Nardini A. & Luglio J. (2014) Leaf hydraulic capacity and drought vulnerability: possible trade-offs and correlations with climate across three major biomes. *Functional Ecology* **28**: 810-818.

Pammenter N.W. & Vander Willigen C. (1998) A mathematical and statistical analysis of the curves illustrating vulnerability of xylem to cavitation. *Tree Physiology* **18**, 589–593.

Paul M.J. & Foyer C.H. (2001) Sink regulation of photosynthesis. *Journal of Experimental Botany* **52**, 1383–1400.

Peng C., Ma Z, Lei X, Zhu Q, Chen H, Wang W, Liu S, Li W, Fang X, & Zhou X. (2011) A drought-induced pervasive increase in tree mortality across Canada's boreal forests. Nature Climate Change **1**, 467-471.

Poyatos R., Aguadé D., Galiano L., Mencuccini M. & Martínez-Vilalta J. (2013) Drought-induced defoliation and long periods of near-zero gas exchange play a key role in accentuating metabolic decline of Scots pine. *New Phytologist,* **200**, 388-401.

Powell T.L., Galbraith D.R., Christoffersen B.O., Harper A., Imbuzeiro H.M.A., Rowland L. et al. (2013) Confronting model predictions of carbon fluxes with measurements of Amazon forests subjected to experimental drought. *New Phytologist* **200**, 350–365.

R Development Core Team (2013) R: A language and environment for statistical computing. R Foundation for Statistical Computing, Vienna, Austria. URL http://www.R-project.org/.

Sala A. (2009) Lack of direct evidence for the carbon-starvation hypothesis to explain drought induced mortality in trees. *Proceedings National Academy of Sciences* USA **106**, E68.

Sala A, Piper F, Hoch G (2010) Physiological mechanisms of drought-induced tree mortality are far from being resolved. *New Phytologist* **186**, 274-281.

De Schepper V, Steppe K (2010) Development and verification of a water and sugar transport model using measured stem diameter variations. *Journal of Experimental Botany* **61**, 2083–2099.

734 Sevanto S., McDowell N.G., Dickman L.T., Pangle R. & Pockman W.T. (2014) How do trees
735 die? A test of the hydraulic failure and carbon starvation hypotheses. *Plant, Cell and Environment*
736 **37**, 153-161.
737 Sperry J.S., Adler F.R., Campbell G.S. & Comstock J.P. (1998) Limitation of plant water use by
738 rhizosphere and xylem conductance: results from a model. *Plant, Cell and Environment* **21**, 347-359.
739 Thornley J.H.M. & Johnson I.R. (1990) *Plant and Crop Modelling: A Mathematical Approach to Plant*
740 *and Crop Physiology*. Oxford: Clarendon Press.
741 Tuzet A., Perrier A. & Leuning R. (2003) A coupled model of stomatal conductance,
742 photosynthesis and transpiration. *Plant, Cell and Environment* **7**, 1097-1116.
743 van Oijen M., Reyer C., Bohn F.J., Cameron D.R., Deckmyn G., Flechsig M., Härkönen
744 S., Hartig F., Huth A., Kiviste A. et al. (2013) Bayesian calibration, comparison and averaging
745 of six forest models, using data from Scots pine stands across Europe. *Forest Ecology and*
746 *Management* **289**, 255-268.
747 von Caemmerer S. & Farquhar G.D. (1981) Some relationships between the biochemistry of
748 photosynthesis and the gas exchange of leaves. *Planta* **153**, 376-387.
749 Venables, W. N. & Ripley, B. D. (2002) *Modern Applied Statistics with S*. Fourth Edition. Springer,
750 New York. ISBN 0-387-95457-0.
751 Vilagrosa A., Hernandez E.I., Luis V.C., Cochard H. & Pausas J.G. (2014) Physiological
752 differences explain the co-existence of different regeneration strategies in Mediterranean
753 ecosystems. *New Phytologist* **201**, 1277-1288.
754 Xu C., McDowell N.G., Sevanto S. & Fisher R.A. (2013) Our limited ability to predict vegetation
755 mortality. *New Phytologist* **200**, 298-300.
756 Wermelinger B., Rigling A., Schneider Mathis D. & Dobbertin M. (2008) Assessing the role of
757 bark- and wood-boring insects in the decline of Scots pine (*Pinus sylvestris*) in the Swiss Rhone
758 valley. *Ecological Entomology* **33**, 239-249.
759 Wright I.J. et al. (2005) Assessing the generality of global leaf trait relationships. *New Phytologist*
760 **166**: 485-496.
761 Zweifel R., Bangerter S., Rigling A. Sterck F.J. (2012) Pine and mistletoes: how to live with a leak
762 in the water flow and storage system? *Journal of Experimental Botany* **63**, 2565-2578.
763

764 **Legends of items in Supporting Information**
765 Table S1. Compilation of datasets of plant hydraulic traits by biome or plant functional types.
766 Notes S1. Sensitivity analysis of model outputs in relation to inputs.
767 Notes S2. Sensitivity analysis of definition of leaf turgor loss point as point of stomatal P50.
768 Figure S1. Illustration of the theoretical relationships used in the model.
769 Table S3. Sensitivity analysis of frequency distribution of failure modes.

770 Table 1. The 11 parameters employed to explore the sensitivity of model structure to the various
771 modes of plant failure to drought. Each parameter is defined, the symbol and the units are given,
772 as well as the central value employed in the simulations and the range of values sampled.

773

Parameter	**Symbol**	**Units**	***50% percentile***	***2.5 and 97.5% percentiles of the distribution sampled***
Maximum xylem hydraulic conductance	K_x	m^3 MPa^{-1} s^{-1}	$2.42*10^{-6}$	$2.21*10^{-7}$ $3.68*10^{-5}$
Maximum phloem hydraulic conductance	K_{ph}	m^3 MPa^{-1} s^{-1}	$1.69*10^{-4}$	$1.86*10^{-5}$ $1.58*10^{-3}$
Water potential Ψ causing 50% loss of K_{xyl}	B_x	MPa	-3.69	-14.38 -1.21
Water potential Ψ causing 50% loss of g_s	B_{gs}	MPa	-0.79	-12.21 -0.11
Maximum photosynthesis	P_{max}	mol s^{-1}	$6.62*10^{-5}$	$6.72*10^{-6}$ $6.02*10^{-4}$
Leaf osmotic pressure at which P goes to zero	c_{max}	MPa	9.24	2.18 60.19
Base respiration rate	R_0	mol s^{-1}	$3.36*10^{-6}$	$1.61*10^{-7}$ $6.05*10^{-5}$
Osmotic pressure above which R begins to increase as a function of c	c_{min}	MPa	1.46	0.22 10.78
Slope of the xylem vulnerability curve	A_x	% PLC MPa^{-1}	2.25	0.11 3.43
Slope of relationship between stomatal conductance and water potential Ψ	A_{gs}	% closure MPa^{-1}	8.09	1.34 30.52
Turgor pressure at the bottom of the phloem	U	MPa	0.63	0.09 3.43

774

775

776 Table 2. The six parameters of the model which were kept fixed in the simulations carried out to
777 explore the sensitivity of model structure to the various modes of plant failure to drought. Each
778 parameter is defined, the symbol and the units are given, as well as the fixed value employed in
779 the simulations.

Parameter	**Symbol**	**Units**	**Central value**
Tree height	h	m	10
Phloem cross-sectional area	A_p	m^2	$1.2*10^{-4}$
Xylem cross-sectional area	A_x	m^2	$2*10^{-3}$
Xylem-phloem radial conductance	K_{rad}	$m^3 Pa^{-1} s^{-1}$	$2*10^{-11}$
Transpiration rate at full stomatal opening	T_0	$m^3 s^{-1}$	$2.25*10^{-6}$
Slope of the photosynthetic response curve to stomatal conductance	γ	-	0.2

780

781

782 Table 3. Results of the general linear model employed to explain xylem P50 as a function of
783 stomatal P50, dataset, biome and plant group. For the datasets based on estimates of turgor loss
784 point (TLP), stomatal P50 was defined here as 70% of TLP (See text for further explanation and
785 Tables S4/S5 for tests using different assumptions) (n=170, R^2_{adj} =0.60). ***, P<0.001.

786

	Degrees freedom	Sum Squares	Mean Square	F value	Prob (>F)
Stomatal P50	1	114.482	114.48	80.79	9.24 e-16***
dataset	5	214.34	42.87	30.25	< 2.2 e-16***
Biome	6	38.146	6.36	4.49	3.26 e-04***
Plant.group	1	51.027	51.03	36.01	1.38 e-08***
Biome * Plant.group	4	53.692	13.42	9.47	7.28 e-07***
Residuals	152	215.384	1.42		

787

788

Figure Legends

Fig 1. Diagrammatic representation of model structure. The two central open tubes indicate xylem and phloem transport (brown and green, respectively). P, photosynthesis; g_s, stomatal conductance; R, respiration, F_{ph}, F_{radial} and F_{xyl}, phloem, radial and xylem transport rates; c_{ph}, phloem osmotic pressure; U_{100}, turgor pressure in unloading element; K_{ph} and K_{xyl}, phloem and xylem conductance; Ψ_{soil} and Ψ_{xyl}, soil and xylem water potential, respectively. Numbers 1 to 100 inside the green (phloem) tube for R refer to the corresponding finite elements of the numerical model. Each of the blow-up circles represents one or more processes or feedbacks that are incorporated in the model. The progressive numbers from 1 to 14 inside the grey circles refer to the 14 processes represented in the model and discussed in the text.

Figure 2. Boxplot distribution of the 11 parameters varied in the model as a function of the three modes of failure (HF = hydraulic failure; CS = carbon starvation; PF = phloem transport failure). Boxplots provide mean and interquartile ranges for each parameter and each mode of failure. The first three boxes on the left in black give the modelled distributions, the last box on the right in red gives the distributions from the empirical data compilations, for those parameters for which empirical data were available. Symbols follow Table 1.

Figure 3. Boxplot distribution of 12 variables calculated at the soil water potentials at which the plants failed, as a function of the three modes of failure (HF = hydraulic failure; CS = carbon starvation; PF = phloem transport failure). Boxplots provide mean and interquartile ranges for each variable and each mode of failure. For each of the three modes of failure, the variable most closely associated with that mode is shown in turquoise in the respective plot (i.e., leaf osmotic potential for PF; xylem PLC for HF; residual flux (or cumulative stores) for CS). Note that the last three variables are plotted on log scale.

Figure 4. Distribution of the model simulations in the space defined by the xylem vulnerability to cavitation (P50) and the stomatal sensitivity to water potentials (stomatal P50) for the three main modes of failure (hydraulic failure, carbon starvation, phloem transport failure). For each panel, the color scheme follows the leaf water potentials at failure (with warmer colors indicating more negative values), following the legend in the first panel.

Figure 5. Distribution of the model simulations in the space defined by xylem P50 and stomatal P50 as per Figure 4. The two main modes of failure (hydraulic failure and carbon starvation) are highlighted with grey and pink points, respectively. Red contour lines indicate 99% relative densities of points for each distribution (e.g., less than 1% of the grey points is located outside

821 the corresponding thick red 1% contour). Red contour distributions are given separately for the
822 grey points (hydraulic failure) and the pink points (carbon starvation). The area of joint
823 occurrence of the two failure modes is therefore indicated by the intersection of the two 1%
824 contour red lines. Turquoise, green, black, red, pink and blue colours indicate boreal, tropical
825 evergreen, tropical seasonal, temperate evergreen, temperate deciduous and dry schlerophyllous
826 biomes, respectively. For each colour, circles indicate angiosperms and squares indicate
827 gymnosperms.

828 Figure 6. A) Distribution of the model simulations in the space defined by the combination of
829 parameters controlling respiration versus those controlling photosynthesis. The pink points
830 indicate the simulations resulting in CS, the black points those resulting in phloem transport
831 failure. Red and black contour lines indicate the respective 99% relative densities of points for
832 each distribution, as per Figure 5. The composite parameter controlling respiration is calculated
833 as $(-R_0/(U^*c_{min})$. The composite parameter controlling photosynthesis is calculated as
834 $P_{max} * B_{gs}/c_{max}$. B). The values of photosynthesis and respiration at failure are given for the runs
835 resulting in CS (pink points) and phloem transport failure (black points). The blue line gives the
836 1:1 line of source-sink balance.

837

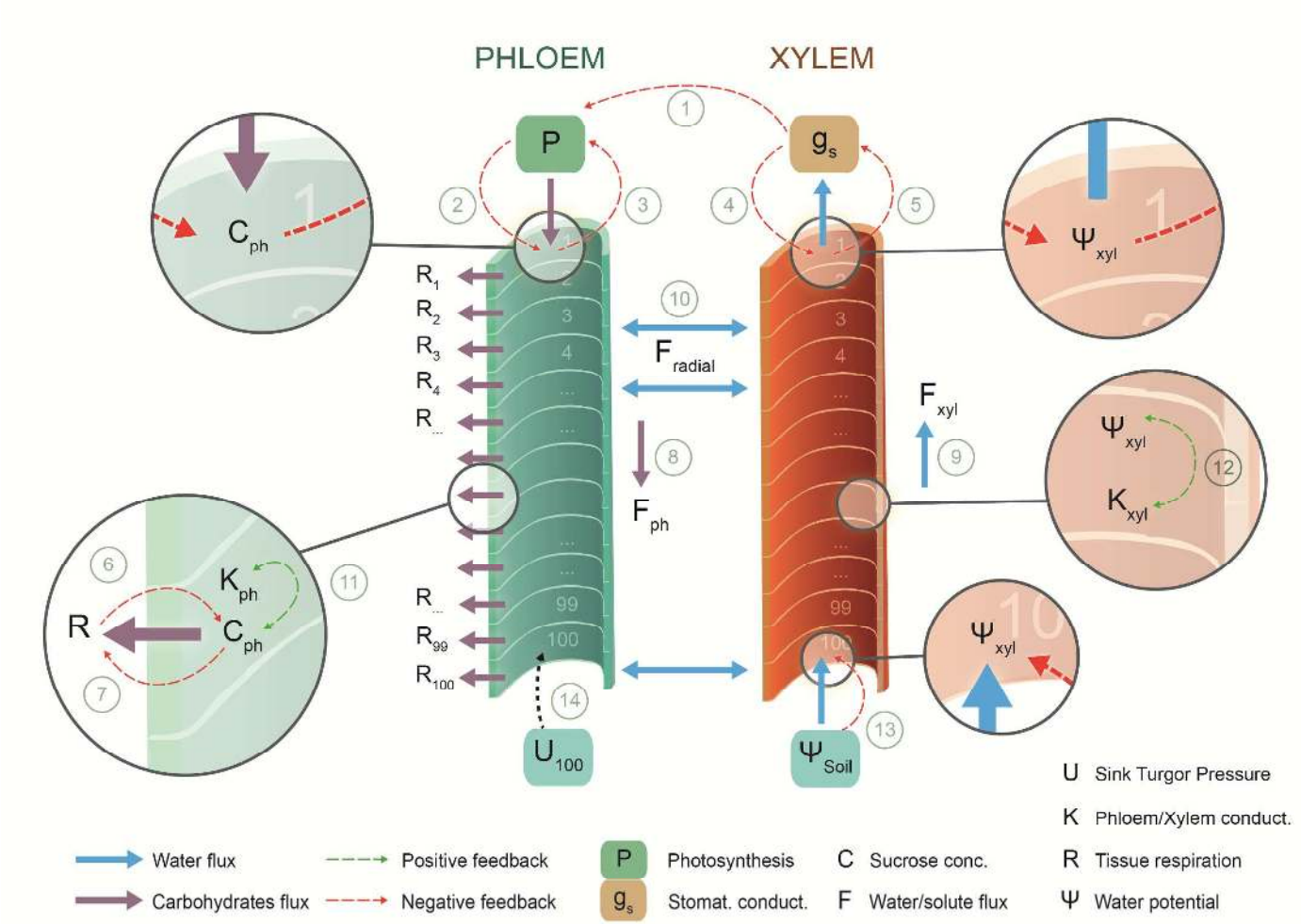
PHLOEM
XYLEM
P
g_s
C_{ph}
Ψ_{xyl}
R_1
R_2
R_3
R_4
$R_{...}$
R_{99}
R_{100}
F_{radial}
F_{ph}
F_{xyl}
K_{ph}
K_{xyl}
R
U_{100}
Ψ_{Soil}
Ψ_{xyl}
Water flux
Carbohydrates flux
Positive feedback
Negative feedback
P Photosynthesis
g_s Stomat. conduct.
C Sucrose conc.
F Water/solute flux
U Sink Turgor Pressure
K Phloem/Xylem conduct.
R Tissue respiration
Ψ Water potential

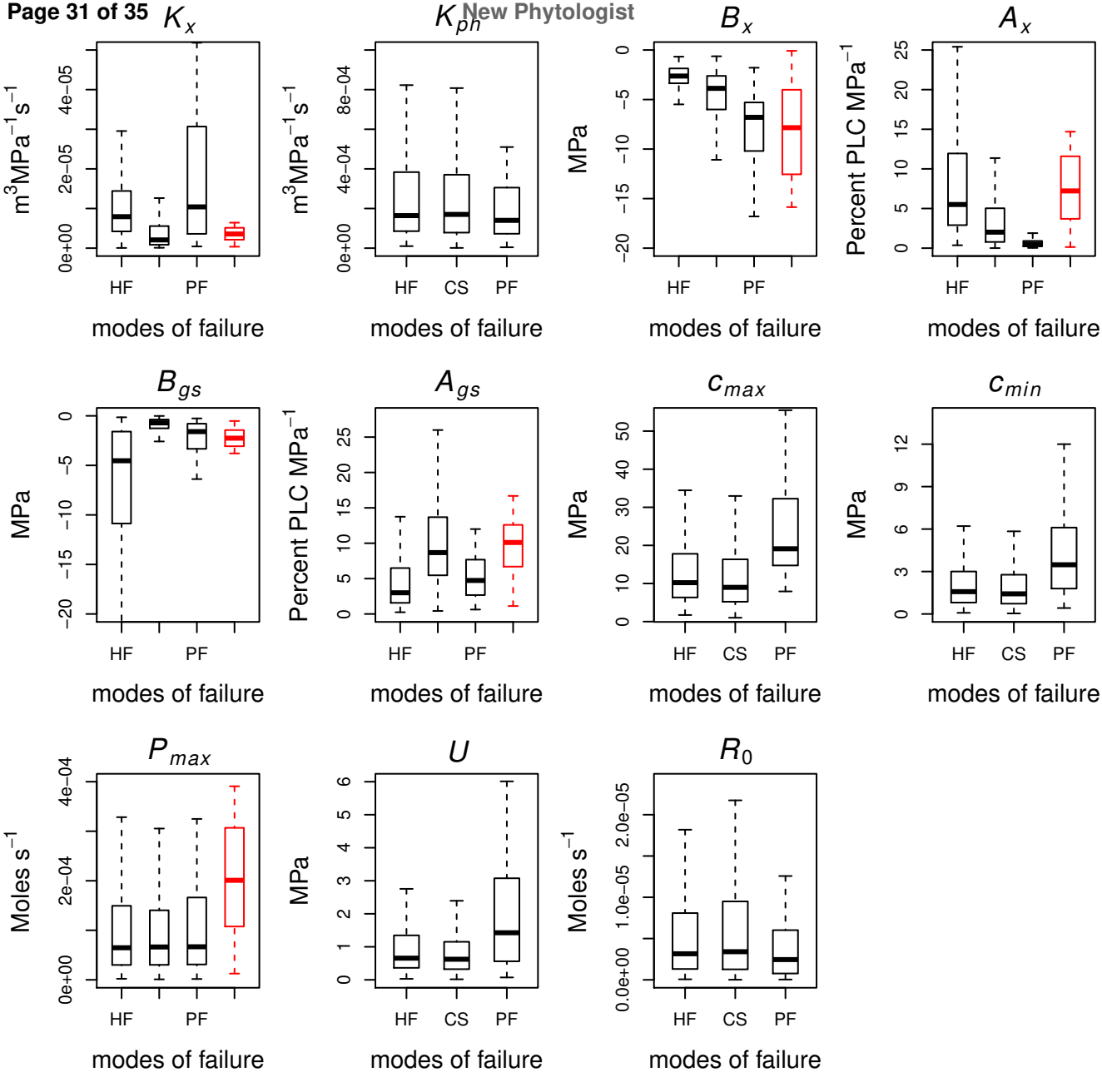
K_x
$m^3MPa^{-1}s^{-1}$
0e+00
2e−05
4e−05
HF
PF
modes of failure
K_{ph}
$m^3MPa^{-1}s^{-1}$
0e+00
4e−04
8e−04
HF
CS
PF
modes of failure
B_x
MPa
0
−5
−10
−15
−20
HF
PF
modes of failure
A_x
Percent PLC MPa^{-1}
0
5
10
15
20
25
HF
PF
modes of failure
B_{gs}
MPa
0
−5
−10
−15
−20
HF
PF
modes of failure
A_{gs}
Percent PLC MPa^{-1}
0
5
10
15
20
25
HF
PF
modes of failure
c_{max}
MPa
0
10
20
30
40
50
HF
CS
PF
modes of failure
c_{min}
MPa
0
3
6
9
12
HF
CS
PF
modes of failure
P_{max}
Moles s^{-1}
0e+00
2e−04
4e−04
HF
PF
modes of failure
U
MPa
0
1
2
3
4
5
6
HF
CS
PF
modes of failure
R_0
Moles s^{-1}
0.0e+00
1.0e−05
2.0e−05
HF
CS
PF
modes of failure

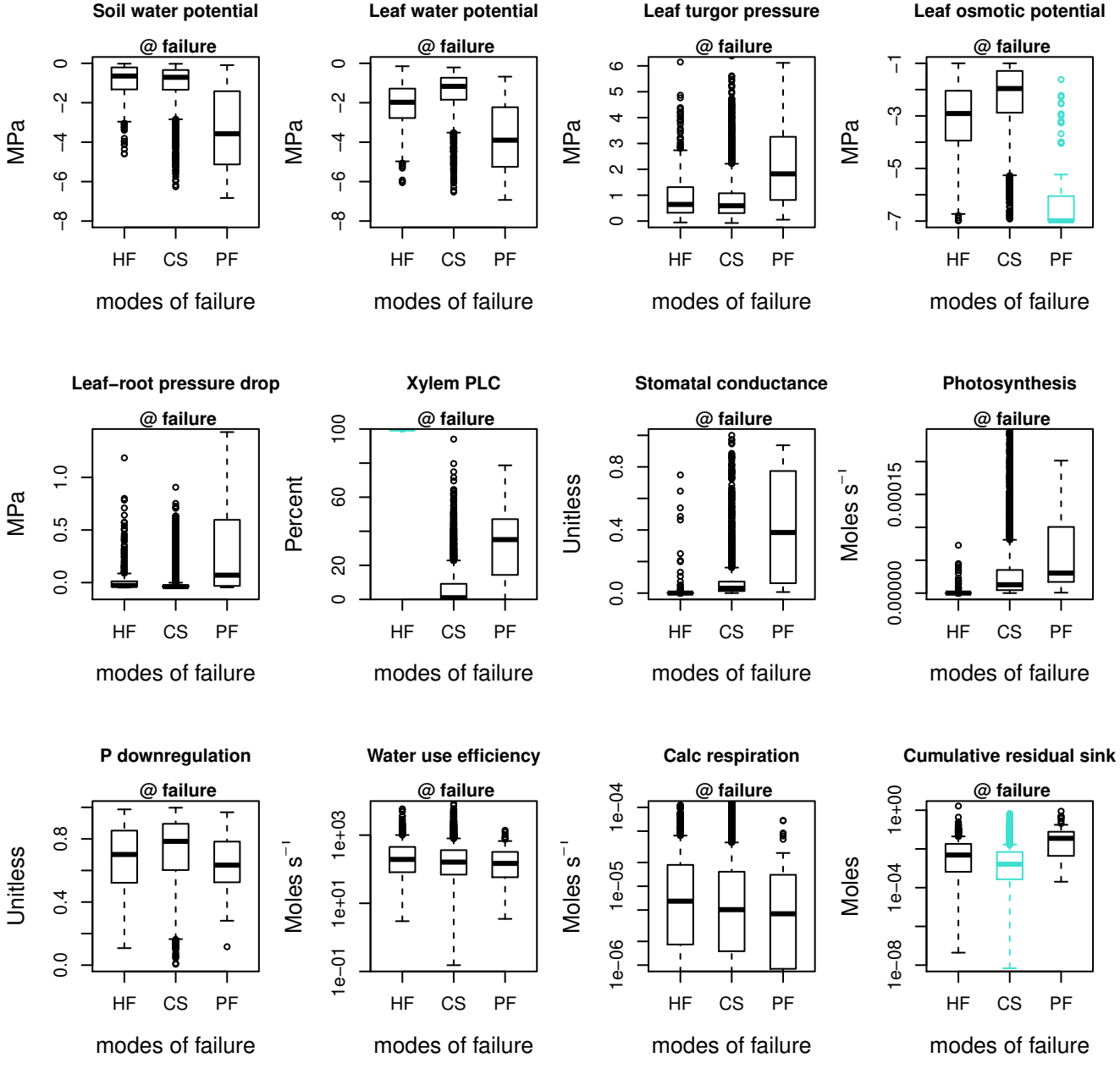
Soil water potential
@ failure
MPa
HF CS PF
modes of failure
Leaf water potential
@ failure
MPa
HF CS PF
modes of failure
Leaf turgor pressure
@ failure
MPa
HF CS PF
modes of failure
Leaf osmotic potential
@ failure
MPa
HF CS PF
modes of failure
Leaf–root pressure drop
@ failure
MPa
HF CS PF
modes of failure
Xylem PLC
@ failure
Percent
HF CS PF
modes of failure
Stomatal conductance
@ failure
Unitless
HF CS PF
modes of failure
Photosynthesis
@ failure
Moles s⁻¹
HF CS PF
modes of failure
P downregulation
@ failure
Unitless
HF CS PF
modes of failure
Water use efficiency
@ failure
Moles s⁻¹
HF CS PF
modes of failure
Calc respiration
@ failure
Moles s⁻¹
HF CS PF
modes of failure
Cumulative residual sink
@ failure
Moles
HF CS PF
modes of failure

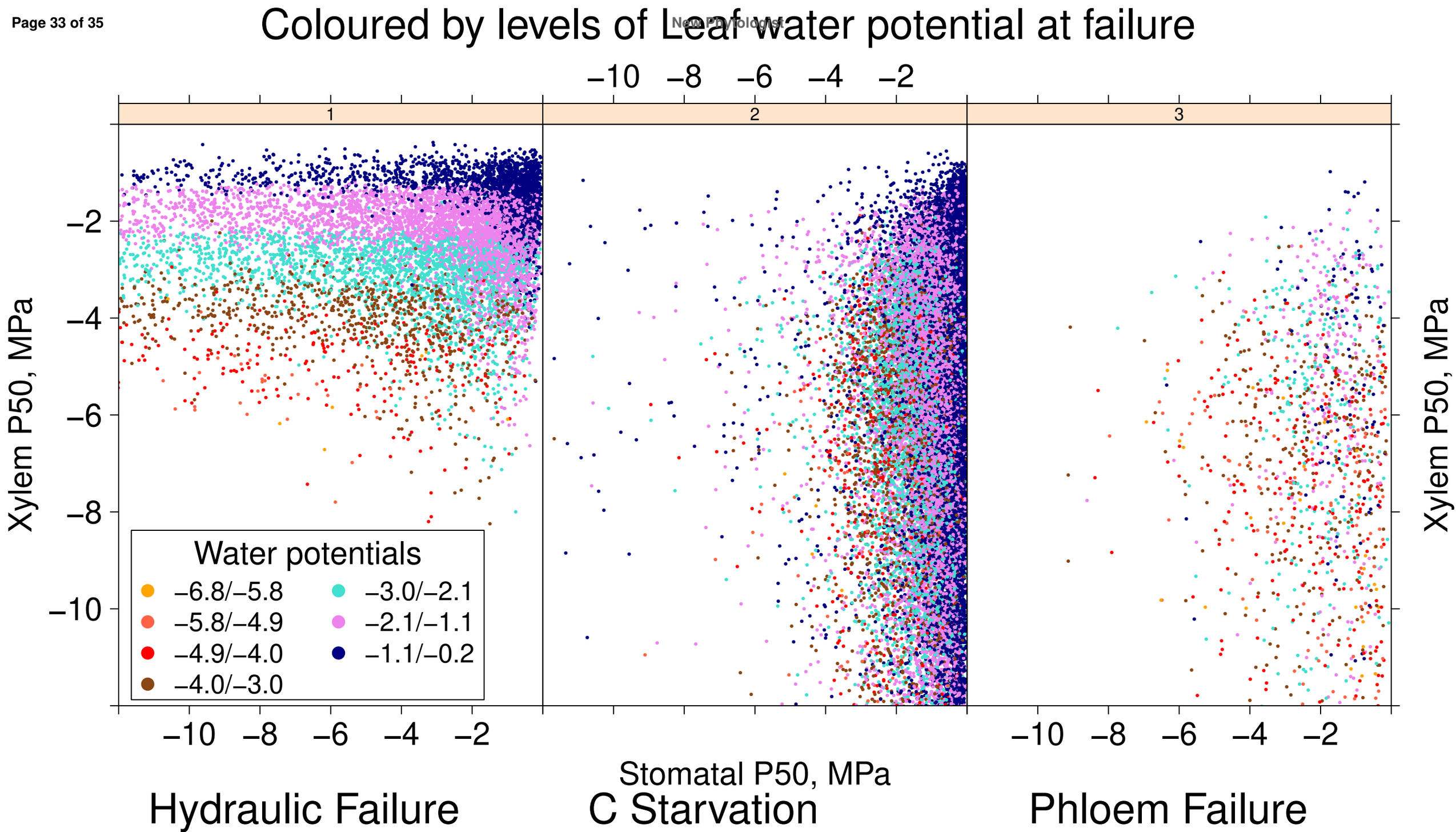
Coloured by levels of Leaf water potential at failure
1
2
3
Xylem P50, MPa
Stomatal P50, MPa
Water potentials
−6.8/−5.8
−5.8/−4.9
−4.9/−4.0
−4.0/−3.0
−3.0/−2.1
−2.1/−1.1
−1.1/−0.2
Hydraulic Failure
C Starvation
Phloem Failure

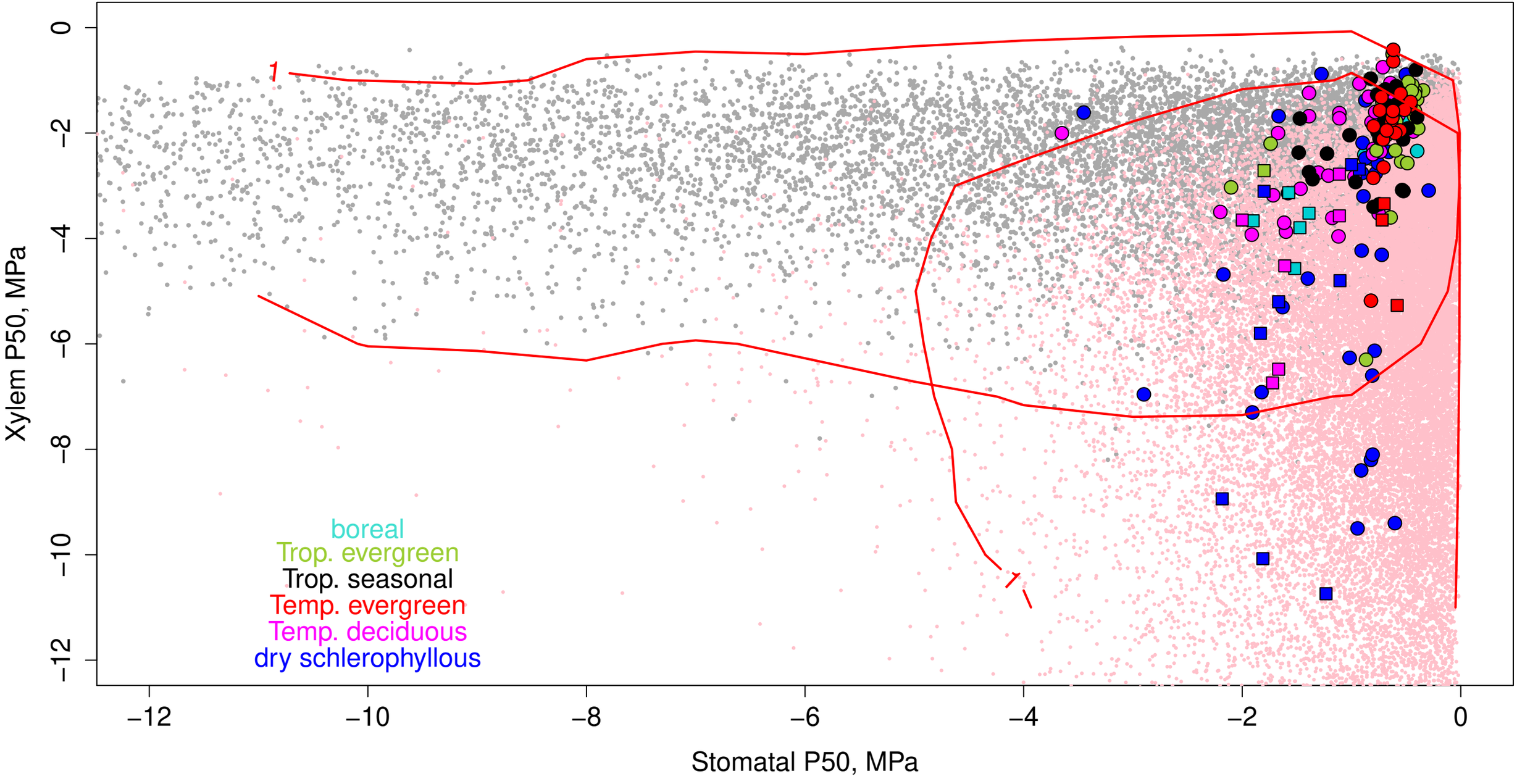
Xylem P50, MPa
0
−2
−4
−6
−8
−10
−12
Stomatal P50, MPa
−12
−10
−8
−6
−4
−2
0
1
1
boreal
Trop. evergreen
Trop. seasonal
Temp. evergreen
Temp. deciduous
dry schlerophyllous

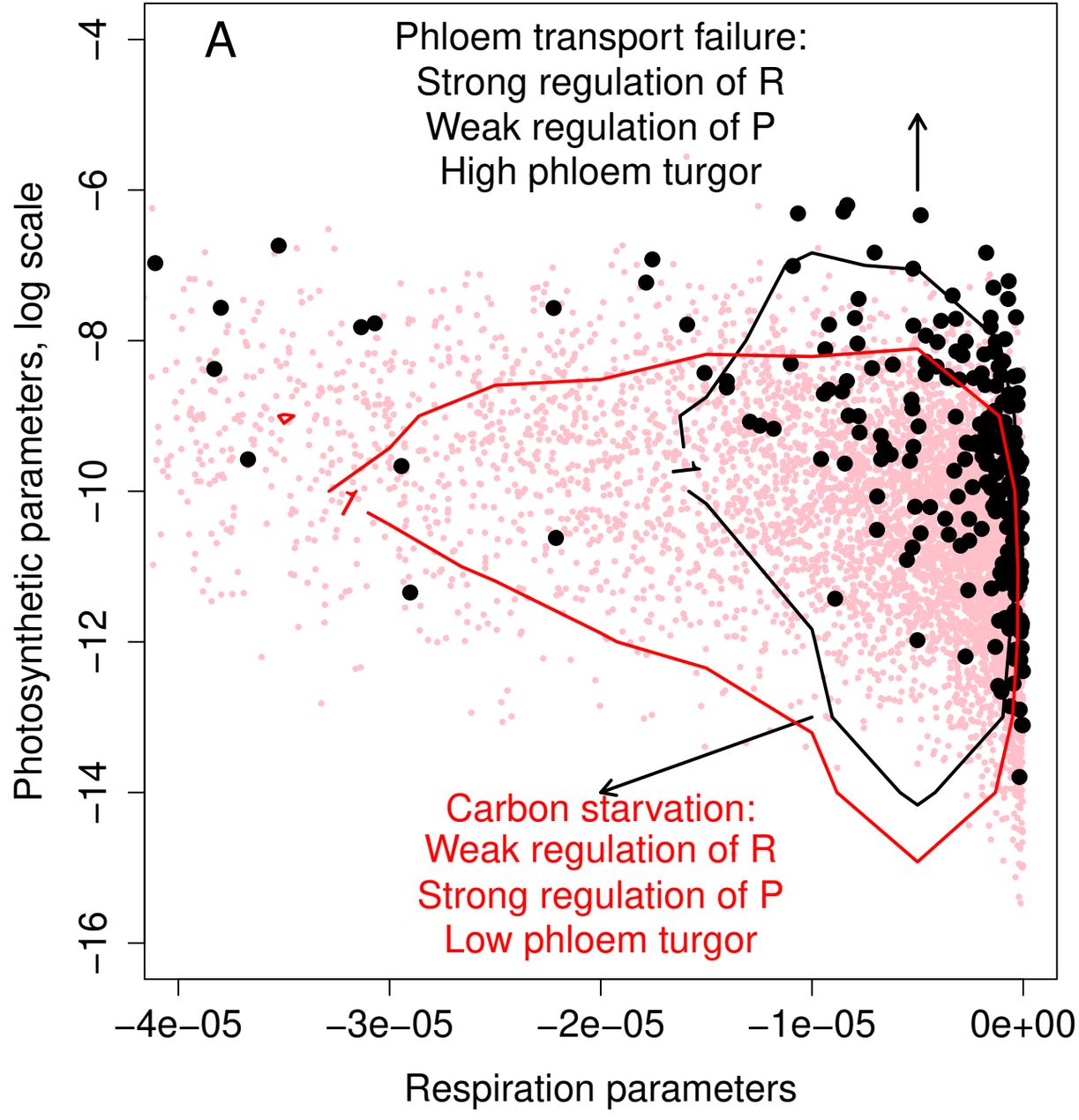
A
Phloem transport failure:
Strong regulation of R
Weak regulation of P
High phloem turgor
Carbon starvation:
Weak regulation of R
Strong regulation of P
Low phloem turgor
Photosynthetic parameters, log scale
−4
−6
−8
−10
−12
−14
−16
−4e−05
−3e−05
−2e−05
−1e−05
0e+00
Respiration parameters

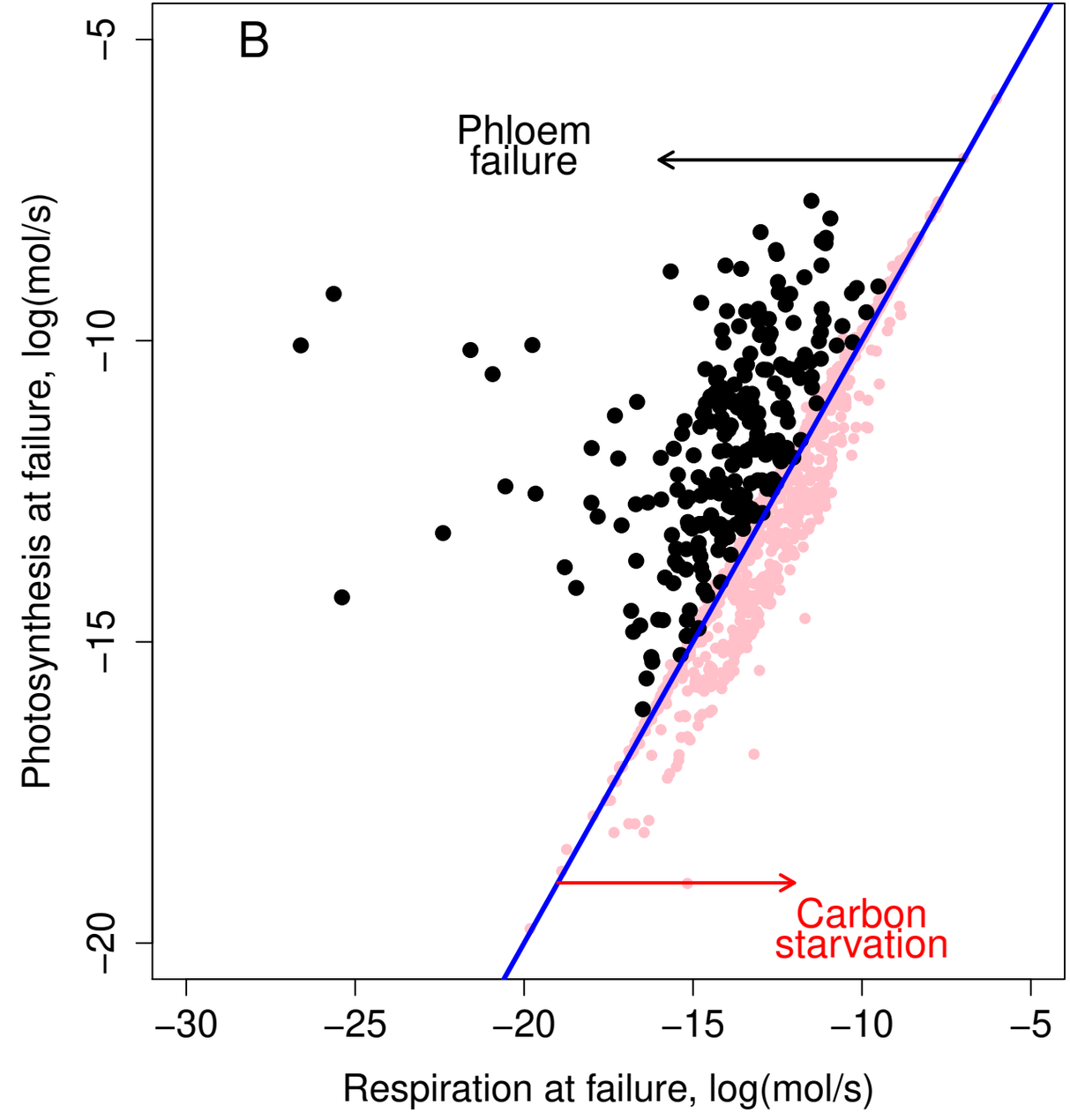
B
Phloem
failure
Carbon
starvation
Photosynthesis at failure, log(mol/s)
−5
−10
−15
−20
−30
−25
−20
−15
−10
−5
Respiration at failure, log(mol/s)